Three-level Dicke quantum battery

Dong-Lin Yang, Fang-Mei Yang, and Fu-Quan Dou *

College of Physics and Electronic Engineering, Northwest Normal University, Lanzhou 730070, China

(Received 27 September 2023; revised 9 June 2024; accepted 13 June 2024; published 26 June 2024)

A quantum battery (QB) is an energy storage and extraction device that is governed by the principles of quantum mechanics. Here we propose a three-level Dicke QB and investigate its charging process by considering three quantum optical states: a Fock state, a coherent state, and a squeezed state. The performance of the QB in a coherent state is significantly superior to that in a Fock or squeezed state. We show that the locked energy is positively related to the entanglement between the charger and the battery, and diminishing the entanglement increases the ergotropy. The role of quantum phase transitions in the charging process of the QB system is analyzed and we find that the behavior of maximum stored energy is jointly determined by ground and excited-state quantum phase transitions. We further demonstrate that, no matter what the initial state is, the stored energy can be completely extracted when N is small ($N = 10$), far below the thermodynamic limit, and the charging power follows a behavior consistent with that of the stored energy.

DOI: 10.1103/PhysRevB.109.235432

I. INTRODUCTION

One of the most promising applications relevant to future quantum technologies is quantum batteries (QBs), i.e., quantum mechanical systems for temporarily storing and then extracting energy [1]. The QB can exploit quantum resources (such as quantum entanglement or quantum coherence) to obtain more efficient work extraction and faster charging processes with respect to classical schemes [2,3]. Considerable attention has been mostly focused on the development of QBs with superior performance [4–18]. It is pivotal to continue research on the construction of QB models [4–11,18–44], the roles of quantum resources [1,6,12,45–63], and the effects of initial states [6,47,64–70] to optimize the performance of QBs. In addition, experimental results have also shown advances towards the exploration of QBs [71–77].

In the quest for high-performance of QBs, efforts have been dedicated to the impact of quantum entanglement in extractable work [4,6,45–47] and charging power [4,5,49,54]. Alicki and Fannes proposed that entangling unitary controls perform better in work extraction capabilities from a QB, when compared to local controls [1]. Entanglement generation can lead to a speedup in the process of work extraction, which was demonstrated in Ref. [49]. Afterward, the collective charging scheme of the ensemble of quantum cells induces a quantum advantage in the charging power [4,5,12]. Another effort is to investigate how the different initial states influence the performance of QBs [6,47,65,70]. A Tavis-Cummings (TC) QB considered three different initial states of the charger and confirmed that the coherent state is optimal for energy extraction in Ref. [6]. Despite such progress, it remains vital to further explore the correlation between entanglement, initial states, and extractable work.

A three-level system interacting with light is related to an important class of quantum optical phenomena, including electromagnetically induced transparency [78,79], lasing without inversion [80,81], as well as methods such as stimulated Raman adiabatic passage (STIRAP) [82,83]. It is desirable to take the three-level system as quantum cells of QBs. A recent work proposed the three-level QB, using the STIRAP technique to bypass the undesired spontaneous discharging and facilitate efficient energy transfer between the ground state and the maximum excited state [18]. Later, a closed-loop three-level QB was introduced where closed-contour interaction can effectively improve the charging performance [27]. Furthermore, a three-level QB utilizing the shortcut to adiabaticity realized highly efficient charging and discharging processes [28]. These works have indicated that, by utilizing the unique structure of three-level systems, more energy can be stored than in two-level systems. Experimentally, three-level QBs based on superconducting circuits were also reported, including the transmon qutrit QB [72] and the Xmon qutrit QB [76].

Another paradigmatic model, in which a collection of two-level systems is coupled to a quantized single-mode light field, called the Dicke model [84], has extensive applications in QBs [5,22,40,71,85,86]. The extension of the two-level Dicke model to the three-level system has been studied [87–101], such as subradiance [87–91], superradiant phase transitions [92–96], time crystalline order [97,98], and enantiodetection of chiral molecules [99]. Encouraged by the new quantum optical phenomena beyond the two-level case in the context of three-level atomic structure, it is natural to inquire whether the implementation of the three-level Dicke model can lead to enhanced performance of QBs.

In this paper, we propose a three-level Dicke QB composed by N Ξ-type three-level atoms and a single-mode cavity. The QB's charging process is discussed with three quantum optical states, i.e., a Fock state, a coherent state, and a squeezed state. We introduce the von Neumann entropy to characterize the entanglement between the charger and the battery and investigate the correlation between the locked energy and the

*Contact author: doufq@nwnu.edu.cn

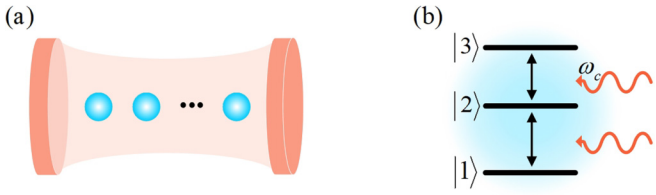

FIG. 1. (a) Sketch of a three-level Dicke QB composed by N identical and independent three-level atoms coupled in a single cavity mode. (b) A Ξ-type three-level atom with three energy levels labeled as $|1\rangle$, $|2\rangle$, and $|3\rangle$, respectively. The transitions $|1\rangle \leftrightarrow |2\rangle$ and $|2\rangle \leftrightarrow |3\rangle$ are mediated by a single cavity mode with frequency ω_c.

entanglement. We are concerned with the dependence of the QB's maximum stored energy and the maximum charging power on the cavity-atom coupling and introduce the quantum phase transitions, Wigner function, and photon distribution to analyze the behavior of the maximum stored energy and ergotropy. In addition, we also analyze the effect of N on the maximum stored energy, maximum charging power, entanglements and ratios. Finally, regardless of the initial state, we show that the stored energy can be fully extracted when $N = 10$, far below the thermodynamic limit.

This paper is organized as follows. Section II introduces the three-level Dicke QB and defines the relevant physical quantities to characterize the behavior of the QB. Then we discuss the charging process of the QB for three different initial states and analyze the influence of the entanglement on the QB in Sec. III. Finally, we give a summary in Sec. IV.

II. MODEL

We consider a QB modeled as N identical and independent Ξ-type three-level atoms coupled to a single-mode cavity, as shown in Fig. 1. The QB system can be described by the following Hamiltonian [87–89,92] ($\hbar = 1$ throughout this paper):

$$H(t) = H_A + H_B + \lambda(t)H_I, \tag{1}$$

where the time-dependent parameter $\lambda(t)$ describes the charging time interval, which we assume to be given by a step function equal to 1 for $t \in [0, T]$ and zero elsewhere. $H_{A,B,I}$ are the Hamiltonians of the charger, battery, and interaction terms, respectively, with the following forms:

$$H_A = \omega_c \hat{a}^\dagger \hat{a}, \tag{2}$$

$$H_B = \sum_{i=1}^{3} \omega_i \hat{A}_{ii}, \tag{3}$$

$$H_I = \frac{g_{12}}{\sqrt{N}}(\hat{a}^\dagger + \hat{a})(\hat{A}_{12} + \hat{A}_{21}) + \frac{g_{23}}{\sqrt{N}}(\hat{a}^\dagger + \hat{a})(\hat{A}_{23} + \hat{A}_{32}). \tag{4}$$

Here $\hat{a}$ ($\hat{a}^\dagger$) annihilates (creates) a photon in the cavity with frequency ω_c. $\hat{A}_{ij} = \sum_{k=1}^{N} |i_k\rangle\langle j_k|$ $(i, j = 1, 2, 3)$ are the collective operators with $|i_k\rangle$ denoting the ith level of the kth atom. The energies of the three states are $\omega_1 < \omega_2 < \omega_3$. g_{ij} is the cavity-atom coupling strength between states $|i\rangle$ and $|j\rangle$. Here, we take into account not only weak coupling strengths, but also coupling strengths that are high enough to reach the regime of ultrastrong coupling (USC) and even deep-strong coupling (DSC). It is well known that the rotating wave approximation (RWA) is no longer valid within the regime of USC. Therefore, we do not consider the RWA, and the introduction of counter-rotating terms gives rise to unexpected physical phenomena. Meanwhile, for simplicity, our QB model also excludes additional terms like the diamagnetic term or the self-polarization term in the USC and DSC regime [102].

We consider the charging process of the three-level Dicke QB in a closed quantum system. The N Ξ-type three-level atoms are prepared in ground state $|1\rangle$ and coupled to a single-mode cavity in the three typical quantum optical states: a Fock state, a coherent state, and a squeezed state, all having the same input energy $2N\omega_c$. Thus, the initial state of the total system is

$$|\Psi(0)\rangle = |\Psi(A)\rangle \otimes |\underbrace{1, 1, \ldots, 1}_{N}\rangle, \tag{5}$$

where $|\Psi(A)\rangle$ is the cavity state with full energy.

In our charging protocol, the QB will start charging when the classical parameter $\lambda(t)$ is nonzero. The wave function of the system evolves with time, i.e.,

$$|\Psi(t)\rangle = U|\Psi(0)\rangle = e^{-iHt/\hbar}|\Psi(0)\rangle. \tag{6}$$

The stored energy of the QB at time t is given by

$$E_B(t) = \mathrm{Tr}[H_B \rho_B(t)], \tag{7}$$

where $\rho_B(t) = \mathrm{Tr}_A[\rho_{AB}(t)]$ is the reduced density matrix of the battery. However, $E_B(t)$ cannot be wholly extracted from the battery, which is known as the second law of thermodynamics. Therefore, a proper measure of the extractable work is provided by the ergotropy [103]:

$$\mathcal{E}_B(t) = E_B(t) - \min_U \mathrm{Tr}[H_B U \rho_B(t) U^\dagger]. \tag{8}$$

Consider the spectral decompositions of the ρ_B and H_B as $\rho_B = \sum_n r_n |r_n\rangle\langle r_n|$ and $H_B = \sum_n \epsilon_n |\epsilon_n\rangle\langle\epsilon_n|$ so that $r_0 \geqslant r_1 \geqslant \cdots$ and $\epsilon_0 \leqslant \epsilon_1 \leqslant \cdots$. The passive counterpart of ρ_B is $\widetilde{\rho} = \sum_n r_n |\epsilon_n\rangle\langle\epsilon_n|$, and its mean energy is unextractable (locked energy) and given by

$$E_{\widetilde{\rho}}(t) = \mathrm{Tr}[H_B \widetilde{\rho}(t)] = \sum_n r_n \epsilon_n. \tag{9}$$

It corresponds to the second term on the right-hand side of Eq. (8), i.e., $\min_U \mathrm{Tr}[H_B U \rho_B(t) U^\dagger] = \sum_n r_n \epsilon_n$. The average charging powers of $E_B(t)$ and $\mathcal{E}_B(t)$ are given by

$$P_B(t) = E_B(t)/t, \tag{10}$$

$$\mathcal{P}_B(t) = \mathcal{E}_B(t)/t. \tag{11}$$

We are interested in exploring the correlation between the entanglement and the ergotropy. Since in our model the quantum state of the total system (charger plus battery) remains pure at all times and the battery state $\rho_B(t)$ will be mixed because of its entanglement with the charger during the time evolution, the entanglement between the charger and battery can be characterized by the *von Neumann entropy* [104–106]

of the battery's reduced density matrix $\rho_B(t)$. The von Neumann entropy is defined by

$$S(t) = -\mathrm{Tr}[\rho_B(t)\log_2 \rho_B(t)]. \tag{12}$$

The ratio between ergotropy and stored energy as another useful quantifier of QB performance is defined as

$$R_B(t) = \mathcal{E}_B(t)/E_B(t). \tag{13}$$

Due to the unitary evolution of the QB system during charging, there will be a reciprocal exchange of energy between the charger and the battery. It may not be necessary to continuously monitor the stored energy, ergotropy, and charging power of the QB throughout the charging process. Therefore, we choose the maximum stored energy $E_{\max}$ (at time t_E), maximum ergotropy $\mathcal{E}_{\max}$ (at time $t_{\mathcal{E}}$), and maximum charging powers $P_{\max}$ (at time t_P) and $\mathcal{P}_{\max}$ (at time $t_{\mathcal{P}}$), to measure QB performance:

$$E_{\max} \equiv \max_t[E_B(t)] = E[(t_E)], \tag{14}$$

$$\mathcal{E}_{\max} \equiv \max_t[\mathcal{E}_B(t)] = \mathcal{E}[(t_{\mathcal{E}})], \tag{15}$$

$$P_{\max} \equiv \max_t[P_B(t)] = P[(t_P)], \tag{16}$$

$$\mathcal{P}_{\max} \equiv \max_t[\mathcal{P}_B(t)] = \mathcal{P}[(t_{\mathcal{P}})]. \tag{17}$$

In addition, the entanglements $\overline{S}_{t_E}$ (at time t_E) and $\overline{S}_{t_P}$ (at time t_P) corresponding to the maximum stored energy and maximum charging power, respectively, are considered. These measures are given by

$$\overline{S}_{t_E} \equiv S(t_E), \tag{18}$$

$$\overline{S}_{t_P} \equiv S(t_P). \tag{19}$$

In what follows, we shall analyze the quantities $E_{\max}$, $\mathcal{E}_{\max}$, $P_{\max}$, and $\mathcal{P}_{\max}$, as well as their ratios

$$\mathcal{R}_e = \mathcal{E}_{\max}/E_{\max} \tag{20}$$

and

$$\mathcal{R}_p = \mathcal{P}_{\max}/P_{\max}. \tag{21}$$

In all subsequent calculations, we choose the energy spectrum of our three-level system as $\omega_1 = 0$, $\omega_2 = 1$, and $\omega_3 = 1.95$. We take ω_c as a dimensionless parameter and let $\omega_c = 1$. Numerical work has been performed by using the PYTHON toolbox QUTIP2 [107].

III. THE CHARGING PROPERTY

In this section, we focus on the charging process of the QB with three initial states of the charger, i.e., a Fock state, a coherent state, and a squeezed state. We then analyze the roles of the entanglement between the charger and the battery. Furthermore, we discuss the asymptotic freedom of the extractable energy and corresponding charging power in the QB.

A. Charging properties and entanglement

In order to analyze the effect of the three different initial states of the charger on the QB, we illustrate the time evolution of the stored energy, ergotropy, and average charging powers as shown in Fig. 2. It demonstrates that when the cavity is in a coherent input state, a QB can achieve higher stored energy, ergotropy, and average charging powers than those achieved with Fock or squeezed input states. The TC QB in Ref. [6] can store more energy in Fock states and extract more energy in coherent states, while the two-photon Jaynes-Cummings QB exhibits better performance in Fock states reported in Ref. [65]. Our result differs from that obtained in Refs. [6,65]. In particular, when the charger is initially in a coherent state, almost all the stored energy of the battery can be extracted to generate valuable work at short times. Therefore, for coherent states, the charging power corresponding to the ergotropy converges to the average storing power in the short term. Furthermore, there is a significant difference between the stored energy and ergotropy over long periods of time for any given initial states of the charger. In comparison to the two-level Dicke QB, the three-level Dicke QB evidently possesses a superior energy storage capacity. This is attributed to the third energy level of three-level atoms, which exhibits an enhanced capability for energy storage. We display the energy level populations in Fig. 7 of Appendix A to illustrate the significance of the third energy level. For different initial states of the cavity, a higher population of the third energy level results in greater energy in the QB.

We investigate the time evolution of the locked energy $E_{\widetilde{\rho}}(t)$, the entanglement $S(t)$, and the ratio $R_B(t)$ for different initial states as shown in Fig. 3. The locked energy and the entanglement show an obvious consistent behavior for all three states. Compared to Fock and squeezed states, coherent states take a longer time to generate more entanglement, which is also reflected in the locked energy. This can be attributed to the fact that a more mixed battery state produces more entanglement between the charger and the battery, leading to an increase in the amount of locked energy, which makes it more difficult to extract the battery energy. When entanglement is relatively small, a coherent state allows for the almost complete extraction of stored energy as valuable work. Moreover, a nearly stable ratio can be achieved across the three different initial states of the charger when entanglement is significant. By comparing Figs. 2(a)–2(c) with Fig. 3, it is desirable to minimize the entanglement between the charger and the battery to maximize the capability of work extraction. Such characteristics indicate that Fock and squeezed states induce a complex and entangling dynamics, resulting in a higher degree of entanglement that may lead to a suppression of extractable energy. Conversely, coherent states may be optimal in the sense of energy extraction because they produce a smaller amount of entanglement, which is consistent with the conclusion demonstrated by Ref. [6].

The results of the maximum stored energy and the maximum charging power of the QB as a function of the cavity-atom coupling strengths g_{12} and g_{23} are shown in Fig. 4. It further shows that the coherent state as the initial state of the charger is the optimal protocol to achieve higher maximum stored energy and maximum charging power. For g_{12} approaching g_{23}, the maximum stored energy exhibits a distinct approximate "triangular" region [depicted by yellow color in Figs. 4(a)–4(c)], within which a critical behavior of energy exists. We further investigate the ground-state [93–96] and excited-state quantum phase transitions (ESQPTs) in the

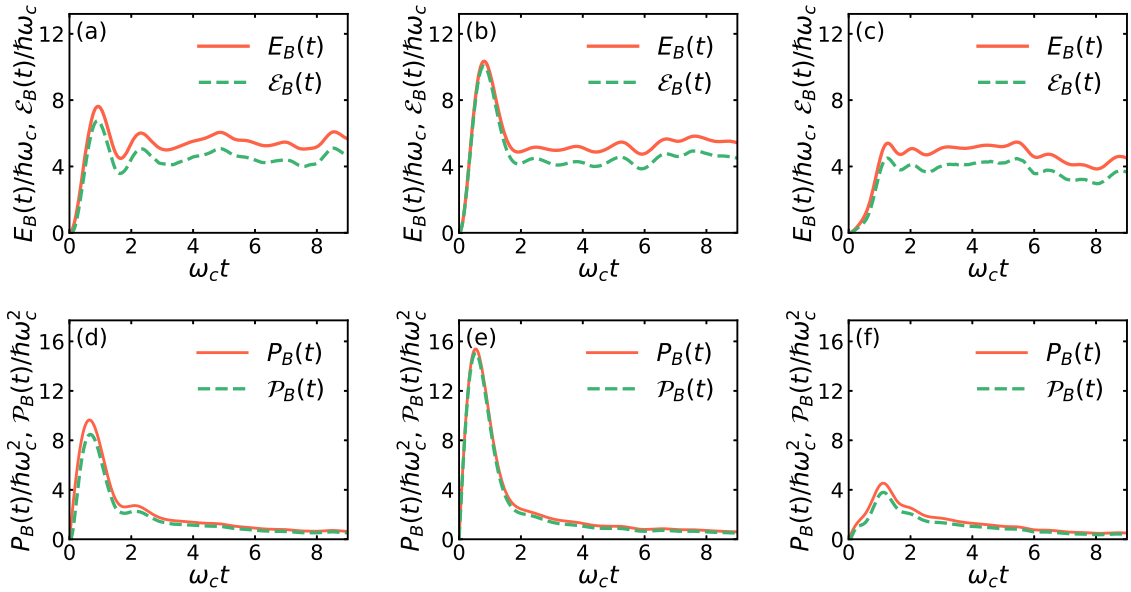

FIG. 2. (a)–(c) The dependence of the stored energy $E_B(t)$ and ergotropy $\mathcal{E}_B(t)$ (both in units of $\hbar\omega_c$) on $\omega_c t$ for three selected states of the charger: a Fock state, a coherent state, and a squeezed state, respectively. (d)–(f) The variation of the average charging powers, $P_B(t)$ and $\mathcal{P}_B(t)$ (both in units of $\hbar\omega_c^2$) on $\omega_c t$ for the same three charger states, respectively. In the following calculations, we use the same settings of $N = 6$, $g_{12} = g_{23} = 1$, unless otherwise specified.

parameter space of couplings g_{12} and g_{23} to explore the physical mechanisms underlying these phenomena (see Appendix A for details). The ground state undergoes quantum phase transitions from the normal phase to the superradiant phase, i.e., from the localized phase to the multifractal phase [see Figs. 8, 9(a)–9(c), and 9(e) of Appendix A]. Near the phase transition point of the ground state, the critical behavior of the maximum stored energy appears. When the energy levels begin to be degenerate, ESQPTs also occur in the QB system. The highest excited state experiences a transition from a localized phase to a multifractal phase [see Figs. 9(a), 9(b), 9(d), and 9(f) of Appendix A]. The triangular region of maximum stored energy appears in the multifractal phase tending

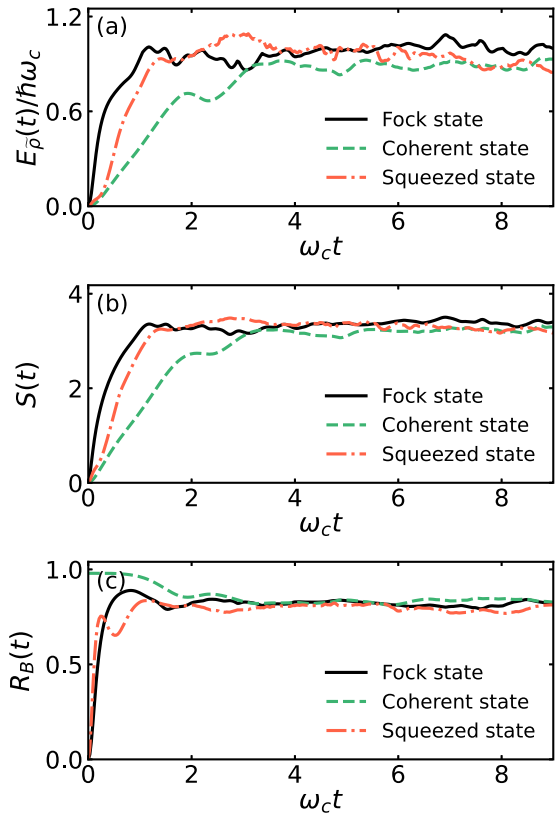

FIG. 3. (a) The locked energy $E_{\tilde{\rho}}(t)$ (in units of $\hbar\omega_c$) as a function of $\omega_c t$ for three initial states of the charger. (b) The entanglement $S(t)$ and (c) the ratio $R_B(t)$ as functions of $\omega_c t$ for the same initial states as in panel (a).

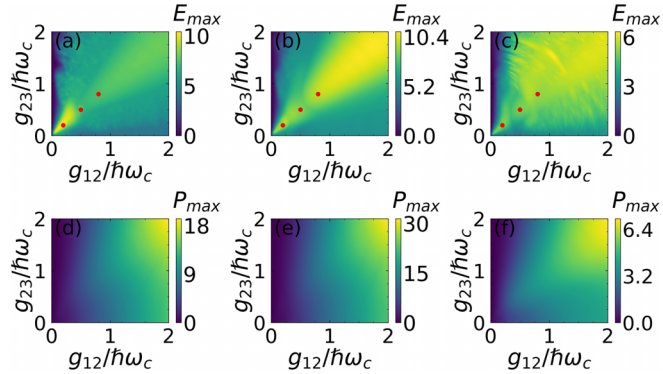

FIG. 4. The contour plots of the QB's maximum stored energy $E_{\max}$ (in units of $\hbar\omega_c$) (a)–(c) and maximum charging power $P_{\max}$ (in units of $\hbar\omega_c^2$) (d)–(f) with different initial states of the charger. The three initial states of charger are as follows: (a), (d) a Fock state, (b), (e) a coherent state, and (c), (f) a squeezed state, respectively. Here, we consider the ranges $g_{12} \in [0, 2]$, $g_{23} \in [0, 2]$. Both g_{12} and g_{23} are in units of $\hbar\omega_c$. The red dots are three randomly selected points near the position where a change of the maximum stored energy occurs. The values of g_{12} and g_{23} for different points are as follows: (0.2, 0.2), (0.5, 0.5), and (0.8, 0.8).

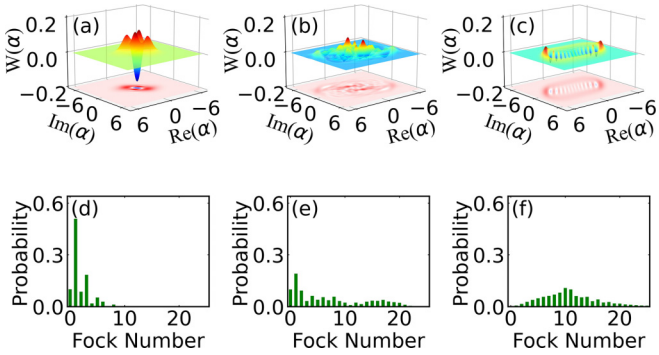

FIG. 5. (a)–(c) Wigner function and (d)–(f) photon distribution in Fock basis corresponding to the maximum stored energy of the charger in Fock states for different cavity-atom coupling strengths. The values of g_{12} and g_{23} are as follows: (a), (d) (0.2, 0.2), (b), (e) (0.5, 0.5), and (c), (f) (0.8, 0.8).

towards perfect delocalization, and is determined by the phase transitions in both the ground state and excited states. In addition, the coupling to achieve maximum energy varies for three different initial states in this region. For a Fock state, the QB can obtain a greater maximum energy storage in the smaller coupling strengths. Conversely, coherent and squeezed states in the larger coupling strengths achieve the higher maximum stored energy. The maximum stored energy and maximum charging power of the QB in the squeezed state are less than those in the other two states. We randomly select three points near the change of the energy within the region. Moreover, stronger cavity-atom coupling strengths in the region increase the maximum charging power for all three initial states of the charger.

To further clarify the behavior of the maximum stored energy and ergotropy, we introduce the Wigner function (see Appendix B for details) and the photon distribution in Fock basis [108–112]. Figure 5 illustrates the cavity Wigner function and photon distribution corresponding to the maximum stored energy in Fock states at three selected points (see Fig. 4). At small cavity-atom coupling strengths, the significantly negative value of the Wigner function indicates the presence of nonclassical properties. The nonclassical properties lead to more charger-battery entanglement and more locked energy, as discussed in Fig. 3. Unlike the probability distribution of coherent and squeezed states in Figs. 10(d) and 11(d), under small coupling, the probability distribution of the Fock state is dominated by odd photons within the range of photon numbers 10, enabling the QB to obtain a higher stored energy. With the coupling further enhanced, the negative value of the Wigner function decreases, and the Wigner function is completely separated into two peaks. This suggests that the properties of the quantum state also change in the region where the maximum energy varies with coupling. The probability becomes more evenly distributed between odd and even number of photons and eventually satisfies a Gaussian profile, which means that the charger can supply more energy to the battery. Similarly, we also calculate the Wigner function and the photon distribution for coherent and squeezed states in Appendix B.

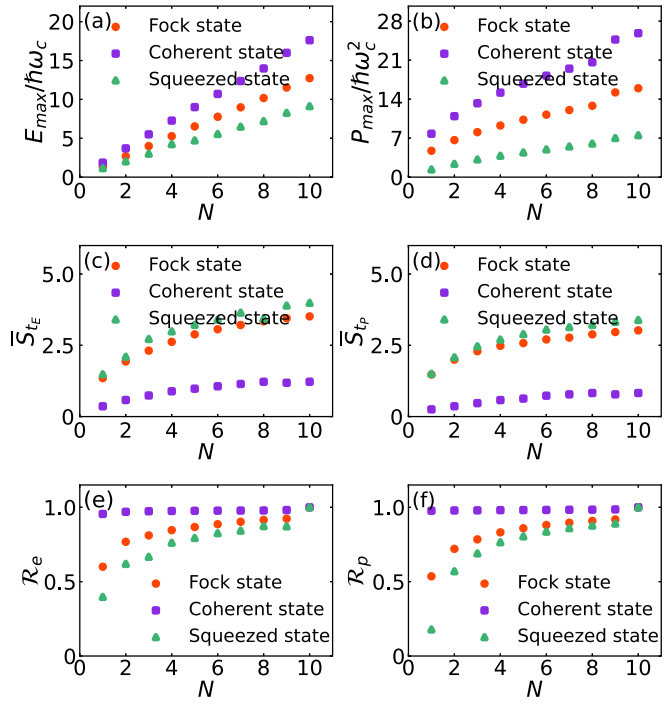

FIG. 6. (a), (b) The maximum stored energy $E_{\max}$ (in units of $\hbar\omega_c$) and the maximum charging power $P_{\max}$ (in units of $\hbar\omega_c^2$) as functions of N for different initial states of the charger, respectively. (c), (d) The entanglements $\overline{S}_{t_E}$ and $\overline{S}_{t_P}$ as functions of N for the same states as in panel (a), individually. (e), (f) The variation of the ratios $\mathcal{R}_e$ and $\mathcal{R}_p$ on N for different initial states the same as in panel (a), respectively. Here, we consider the ranges $N \in [0, 10]$.

B. Asymptotic freedom

We have investigated how the entanglement and cavity-atom coupling strengths affect the charging process of the QB when the number of batteries is fixed for three initial states of the charger. Hereafter, we will analyze the effect of the entanglement on the QB's performance as the number N of three-level atoms increases.

In Fig. 6, we display the maximum stored energy $E_{\max}$, the maximum charging power $P_{\max}$, the entanglements $\overline{S}_{t_E}$ and $\overline{S}_{t_P}$, and the ratios $\mathcal{R}_e$ and $\mathcal{R}_p$ as a function of N for three initial states of the charger. With a coherent state as the initial state for the charger, the QB can obtain a greater maximum stored energy and a higher maximum charging power as N increases, while maintaining a smaller entanglement between the charger and the battery than Fock and squeezed states. We naturally conclude that the entanglement is the main limiting factor in improving the QB's performance for three initial states of the charger. Particularly, the entanglement entropy of the subsystem presents a notable characteristic: it grows logarithmically with the size of the battery, thereby adhering to an *area law* [113–115]. However, the stored energy scales linearly with the battery's size. Therefore, we expect that the energy locked up by the entanglement will become negligible compared to the stored energy as N approaches infinity. When the number of three-level atoms N is small and the initial state of the charger is either a Fock or a squeezed state, the locked energy occupies a larger proportion of the stored

energy in the battery. Consequently, the extractable energy from the battery is much less than the stored energy, and the fraction of charging power corresponding to the extractable energy is also notably low when N is small [see Figs. 6(e) and 6(f)]. The coherent state produces less entanglement than the Fock and squeezed states, leading to the lower locked energy. Therefore, the coherent state has a higher extractable energy and correspondingly higher charging power even at small N. As N increases, the locked energy becomes much smaller relative to the stored energy, resulting in a larger extractable energy in the battery for Fock and squeezed states. Interestingly, regardless of the initial state of the charger, the energy stored in the QB can be completely extracted when $N = 10$, and the behavior of the charging power aligns with the energy as well. This is attributed to the energy storage and extraction advantage of the three-level Dicke model, which is distinct from the two-level model. On the one hand, in the two-level TC QB and Dicke QB discussed in Ref. [6], when $N = 10$, energy extraction is higher in the coherent state but lower in the Fock and squeezed states. However, for different states, the three-level Dicke QB allows full energy extraction even when N is small ($N = 10$), without reaching the thermodynamic limit. On the other hand, the three-level Dicke QB stores and extracts more energy than the two-level QB. As N gradually increases and even reaches the thermodynamic limit, although the two-level QB also achieves higher energy extraction efficiency, the three-level Dicke QB still stores and extracts more energy, far exceeding that of the two-level QB under the same number of atoms and initial state. Therefore, the three-level Dicke QB outperforms the two-level Dicke QB in energy storage and extraction. We also argue that as the size of our battery continues to grow, the extractable energy will converge to the stored energy, and the charging power associated with the ergotropy will also approach the average storing power.

IV. CONCLUSIONS

We have introduced the concept of the three-level Dicke QB, consisting of N identical and independent Ξ-type three-level atoms coupling to a single-mode cavity. We have analyzed the influence of three quantum optical states (Fock, coherent, and squeezed states) of the charger on the performance of QBs, including the stored energy, ergotropy, and average charging power. Our results show that the coherent state can significantly enhance the charging performance compared to the Fock and squeezed states. The locked energy and the entanglement between the charger and the battery exhibit consistent behavior, indicating that entanglement is the main limiting factor in the capability of work extraction. When the level of entanglement is relatively low, a coherent state can almost completely extract the stored energy at short times. The effect of the cavity-atom coupling strengths on the maximum stored energy and the maximum charging power depends on the initial states of the charger. By analyzing the quantum phase transitions, Wigner function, and photon distribution, we have explained the behavior of the maximum stored energy and ergotropy. We have also investigated how the number N influences the maximum stored energy, maximum charging power, entanglements, and ratios. The coherent state leads to a greater maximum stored energy and maximum charging power, while also maintaining a lower entanglement than the Fock and squeezed states. We have found that when $N < 10$, for the charger either in the Fock or the squeezed state, the ergotropy can be less than the energy stored in the battery. The fraction of charging power corresponding to the ergotropy is also low and the coherent state is the optimal initial state. When N approaches 10, almost all of the stored energy in the battery can be extracted. No matter what the initial state is, all of the stored energy becomes extractable for a small N ($N = 10$), which is much less than the thermodynamic limit ($N \to \infty$), and the charging power follows the same trend. Our paper demonstrates that the extractable energy and corresponding charging power in the QB is asymptotically free as N continues to grow.

ACKNOWLEDGMENTS

We thank the anonymous reviewers for valuable comments and suggestions. This work is supported by the National Natural Science Foundation of China (Grant No. 12075193).

APPENDIX A: ENERGY LEVEL POPULATIONS AND QUANTUM PHASE TRANSITIONS

We investigate the time evolution of the energy level populations for different initial states as shown in Fig. 7. It demonstrates that the third energy level is crucial for the

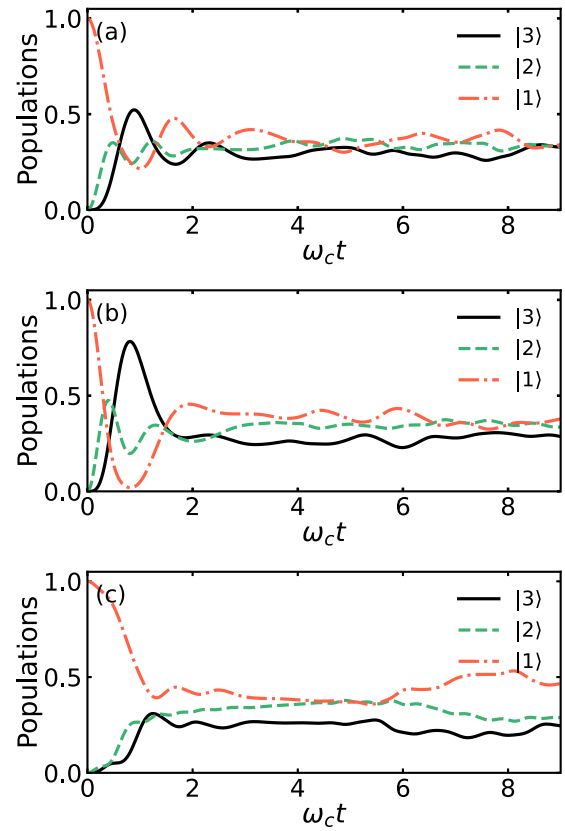

FIG. 7. The energy level populations as a function of $\omega_c t$ for three initial states of the charger: (a) Fock state, (b) coherent state, and (c) squeezed state.

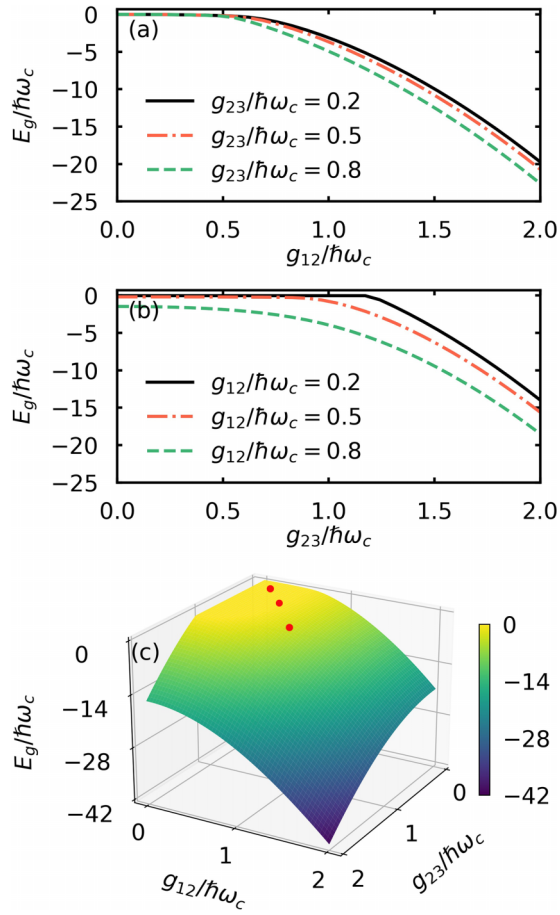

FIG. 8. (a) The dependence of the ground-state energy E_g (in units of $\hbar\omega_c$) on cavity-atom coupling strength g_{12} (in units of $\hbar\omega_c$). (b) The dependence of E_g (in units of $\hbar\omega_c$) on g_{23} (in units of $\hbar\omega_c$). (c) The ground-state energy E_g (in units of $\hbar\omega_c$) varies with the coupling strengths g_{12} and g_{23} (both in units of $\hbar\omega_c$). The values of g_{12} and g_{23} for three red points are as follows: (0.2, 0.2), (0.5, 0.5), and (0.8, 0.8).

three-level Dicke QB. In a coherent state, the population of the third level is much higher than that in Fock and squeezed states. Therefore, the QB in a coherent state can store more energy.

Figures 8(a) and 8(b) display the ground-state energy E_g as a function of the cavity-atom coupling strengths g_{12} and g_{23}, respectively. There are quantum phase transitions from normal phases ($E_g = 0$) to superradiant phases ($E_g < 0$) in the QB system. When the values of the coupling strengths g_{12} and g_{23} are $(0.5, 0.5)$, the quantum phase changes significantly. We also calculate the ground-state energy with the variations of coupling strengths g_{12} and g_{23}, as shown in Fig. 8(c). With the increase of coupling strengths, the ground-state energy gradually decreases to a negative value, further demonstrating the existence of a quantum phase transition from the normal phases to the superradiant phases.

Here, we discuss the ESQPTs by considering the eigenvalue and eigenstate properties [116–121]. Previous works have investigated the ESQPTs using various methods, such as the energy spectrum, consecutive level spacing ratio [122], von Neumann entanglement entropy [123], concurrence [124], participation ratio (PR) [125], and multifractal dimension [126,127]. Here, we choose the energy spectrum, PR, and multifractal dimension to characterize the ESQPTs in our QB system. Initially, PR is defined as a measure of the localization of quantum states, and recent work has linked PR to ESQPTs [119,121]. An arbitrary eigenstate $|\psi\rangle$ can be decomposed into a set of bases in the full Hilbert space of our QB system. The basis is denoted as $|j\rangle = |n\rangle \otimes |m\rangle$ with amplitudes ψ_j, where $|n\rangle$ represents the bosonic basis states and $|m\rangle$ represents the atomic basis states. Thus $|\psi\rangle = \sum_j^{N_D} \psi_j |j\rangle$, where N_D represents the dimensions of the entire Hilbert space. The PR of this eigenstate is defined as

$$\mathrm{PR} = \frac{1}{\sum_{j=1}^{N_D} |\psi_j|^4}. \tag{A1}$$

To further elucidate the quantum phase transitions, we introduce the concept of multifractal dimension [126,127]. When the Hilbert space dimension N_D is large, the multifractal dimension of the eigenstate $|\psi\rangle$ can be represented as

$$D_q = \frac{S_q}{\ln(N_D)}, \tag{A2}$$

where $S_q = \frac{1}{1-q} \ln\left(\sum_{j=1}^{N_D} |\psi_j|^{2q}\right)$ is the q-dependent participation entropy for $q \in \mathbb{R}^+$. In the Shannon limit ($q = 1$), $S_1 = \sum_j |\psi_j|^2 \ln\left(|\psi_j|^2\right)$, while the case $q = 2$ is related to the usual PR with $S_2 = -\ln[(\mathrm{PR})^{-1}]$ [127]. For a perfectly delocalized state, $S_q = \ln(N_D)$ and $D_q = 1$ for all q. In contrast, if a state is localized, $S_q = \text{const}$ and $D_q = 0$. In an intermediate situation, wave functions are extended but nonergodic with $S_q = D_q \ln(N_D)$ where $0 < D_q < 1$ and the state is multifractal [119,127]. In our calculations, we take $q = 1$.

The energy spectra as functions of g_{12} and g_{23}, respectively, are shown in Figs. 9(a) and 9(b). We can obtain ground-state quantum phase transitions from the normal phase to the superradiant phase at the lowest energy level of the energy spectrum. Different energy levels degenerate as the coupling becomes stronger around $E_n = 0$. The energy spectrum presents ESQPTs signaled by singularities in the energy level structure (the point at which the energy levels begin to be degenerate) [128]. We calculate the PR and D_1 for the ground state as a function of g_{12} and g_{23}, shown in Figs. 9(c) and 9(e). The ground-state PR and D_1 clearly show the normal-superradiant phase transitions, similar to the behavior in Fig. 8(c). In the normal phase $D_1 = 0$, indicating that the ground state is localized in the normal phase. Contrastingly in the superradiant phase $0 < D_1 < 1$ and hence the superradiant phase is neither perfectly delocalized nor localized, but actually exhibits multifractal character [127]. As mentioned previously, there is a critical behavior within the approximate triangular region for the maximum stored energy, and this behavior appears under the coupling range of the ground-state phase transitions. Figures 9(d) and 9(f) illustrate the dependence of the highest eigenstate PR and D_1 on g_{12} and g_{23}. The excited-state PR and D_1 exhibit a distinct approximate triangular region (yellow region of PR and D_1), and this feature will be evident in the maximum stored energy shown in Figs. 4(a)–4(c). When the coupling strengths g_{12} and g_{23} are very small, $D_1 = 0$, the excited state is localized. As the coupling increases, when the difference between g_{12}

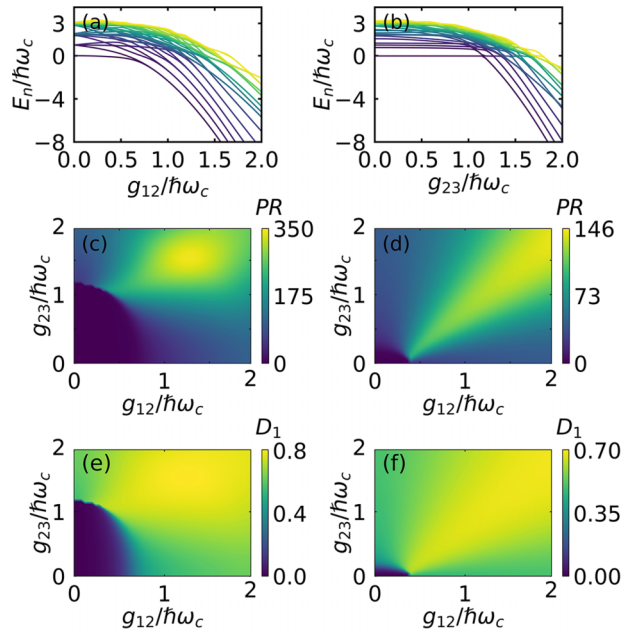

FIG. 9. (a) Energy spectrum E_n (in units of $\hbar\omega_c$) as a function of g_{12} (in units of $\hbar\omega_c$) with $g_{23} = 0.2$. (b) Energy spectrum E_n (in units of $\hbar\omega_c$) as a function of g_{23} (in units of $\hbar\omega_c$) with $g_{12} = 0.2$. The energy spectrum is obtained by computing the first 50 eigenvalues of the QB system. Participation ratio for the ground state (c) and highest eigenstate (d) of the QB system as a function of g_{12} and g_{23}. Multifractal dimension D_1 for the ground state (e) and highest eigenstate (f) of the QB system as a function of g_{12} and g_{23}. For simplicity, we take $N = 4$ in these calculations.

and g_{23} is large (green regions of D_1), $0 < D_1 < 1$, the region behaves like a multifractal phase. For g_{12} close to g_{23} (depicted by the yellow color of D_1), the value of D_1 increases and the excited state is also multifractal, further tending to the delocalized phase. Although we choose the highest eigenstate to characterize the ESQPTs, the quantum phase transitions are also present in other highly excited states, as can be seen from the energy spectrum. Therefore, the approximate triangular region where the maximum stored energy appears is jointly determined by the quantum phase transitions of the ground state and a series of highly excited states. The phase transitions of both the ground state and excited states collectively influence the charging properties. It is noticed that the behavior of the energy spectrum, PR, and D_1 does not significant change for ground state and excited state as N increases.

APPENDIX B: WIGNER FUNCTION AND PHOTON DISTRIBUTION IN COHERENT AND SQUEEZED STATES

A convenient way to visualize a quantum state is through the Wigner function using the phase-space formalism [108], which can be defined as the Fourier transform of the symmetrically ordered characteristic function $\chi(\eta)$:

$$W(\alpha) = \frac{1}{\pi^2}\int \exp(\eta^*\alpha - \eta\alpha^*)\chi(\eta)d^2\eta, \tag{B1}$$

where α is an arbitrary point in phase space. The symmetrically ordered characteristic function $\chi(\eta)$ is

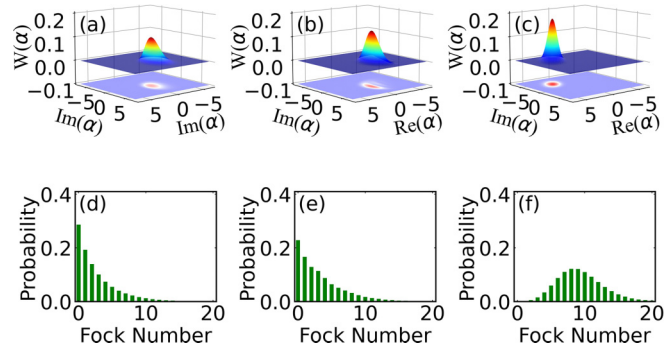

FIG. 10. (a)–(c) Wigner function and (d)–(f) photon distribution in Fock basis corresponding to the maximum stored energy of the charger in coherent states for different cavity-atom coupling strengths. The values of g_{12} and g_{23} are as follows: (a), (d) (0.2, 0.2), (b), (e) (0.5, 0.5), and (c), (f) (0.8, 0.8).

given by

$$\chi(\eta) = \mathrm{Tr}\{\rho_A e^{\eta\hat{a}^\dagger - \eta^*\hat{a}}\}, \tag{B2}$$

where ρ_A is the reduced density matrix of the charger in our calculations. The Wigner function can also be defined in terms of the generalized conjugate position x and momentum p as $\bar{W}(x,p) = \frac{1}{\pi\hbar}\int_{-\infty}^{\infty}\langle x+z|\rho_A|x-z\rangle e^{-2ipz/\hbar}dz$, and $W(\alpha)$ can be derived from $\bar{W}(x,p)$. We calculate the Wigner function and photon distribution corresponding to the maximum stored energy for the charger in coherent and squeezed states, as shown in Figs. 10 and 11, respectively. Initially, the Wigner function of the coherent state is positive, indicating that the state displays a semiclassical nature. As previously discussed, the entanglement generated between the charger and the battery is relatively minor for this state. With the coupling strengths increasing, the Wigner function shows "ripples" and the photon distribution extends towards larger photon numbers. This ripple pattern indicates a change in the quantum state at that moment. At the same time, the maximum energy of the coherent state near this coupling strength undergoes a significant change. At stronger coupling, the Wigner function transforms into an oval shape, and the photon probability distribution follows a Gaussian profile. This allows the charger

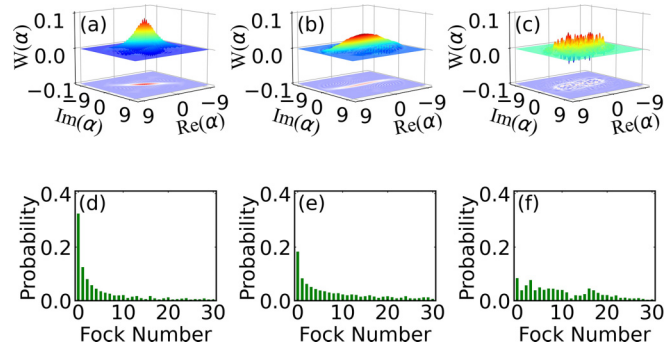

FIG. 11. (a)–(c) Wigner function and (d)–(f) photon distribution in Fock basis corresponding to the maximum stored energy of the charger in squeezed states for different cavity-atom coupling strengths. The values of g_{12} and g_{23} are as follows: (a), (d) (0.2, 0.2), (b), (e) (0.5, 0.5), and (c), (f) (0.8, 0.8).

to deliver more energy to the battery and the QB to achieve a higher maximum stored energy. The squeezed state is similar to the Fock state in that the Wigner function has a negative value and it is also a highly nonclassical state. Its Wigner function displays prominent oscillatory behavior. The oscillatory and negative values of the Wigner function become more pronounced under strong coupling. Similarly, in the approximate triangular region, near the coupling where a significant change in the maximum energy occurs, the Wigner function undergoes variations. The photon distribution in the squeezed state oscillates under strong coupling, resulting in minimal stored energy in comparison to the Fock and coherent states.

[1] R. Alicki and M. Fannes, Entanglement boost for extractable work from ensembles of quantum batteries, Phys. Rev. E **87**, 042123 (2013).

[2] F. Campaioli, F. A. Pollock, and S. Vinjanampathy, Quantum batteries, *Thermodynamics in the Quantum Regime* (Springer, New York, 2018), pp. 207–225.

[3] F. Campaioli, S. Gherardini, J. Q. Quach, M. Polini, and G. M. Andolina, Colloquium: Quantum batteries, arXiv:2308.02277.

[4] F. C. Binder, S. Vinjanampathy, K. Modi, and J. Goold, Quantacell: Powerful charging of quantum batteries, New J. Phys. **17**, 075015 (2015).

[5] D. Ferraro, M. Campisi, G. M. Andolina, V. Pellegrini, and M. Polini, High-power collective charging of a solid-state quantum battery, Phys. Rev. Lett. **120**, 117702 (2018).

[6] G. M. Andolina, M. Keck, A. Mari, M. Campisi, V. Giovannetti, and M. Polini, Extractable work, the role of correlations, and asymptotic freedom in quantum batteries, Phys. Rev. Lett. **122**, 047702 (2019).

[7] G. M. Andolina, D. Farina, A. Mari, V. Pellegrini, V. Giovannetti, and M. Polini, Charger-mediated energy transfer in exactly solvable models for quantum batteries, Phys. Rev. B **98**, 205423 (2018).

[8] G. M. Andolina, M. Keck, A. Mari, V. Giovannetti, and M. Polini, Quantum versus classical many-body batteries, Phys. Rev. B **99**, 205437 (2019).

[9] T. P. Le, J. Levinsen, K. Modi, M. M. Parish, and F. A. Pollock, Spin-chain model of a many-body quantum battery, Phys. Rev. A **97**, 022106 (2018).

[10] D. Rossini, G. M. Andolina, and M. Polini, Many-body localized quantum batteries, Phys. Rev. B **100**, 115142 (2019).

[11] F. Pirmoradian and K. Mølmer, Aging of a quantum battery, Phys. Rev. A **100**, 043833 (2019).

[12] F. Campaioli, F. A. Pollock, F. C. Binder, L. Céleri, J. Goold, S. Vinjanampathy, and K. Modi, Enhancing the charging power of quantum batteries, Phys. Rev. Lett. **118**, 150601 (2017).

[13] N. Friis and M. Huber, Precision and work fluctuations in Gaussian battery charging, Quantum **2**, 61 (2018).

[14] D. Farina, G. M. Andolina, A. Mari, M. Polini, and V. Giovannetti, Charger-mediated energy transfer for quantum batteries: An open-system approach, Phys. Rev. B **99**, 035421 (2019).

[15] Y.-Y. Zhang, T.-R. Yang, L. Fu, and X. Wang, Powerful harmonic charging in a quantum battery, Phys. Rev. E **99**, 052106 (2019).

[16] R. Alicki, A quantum open system model of molecular battery charged by excitons, J. Chem. Phys. **150**, 214110 (2019).

[17] F. Mazzoncini, V. Cavina, G. M. Andolina, P. A. Erdman, and V. Giovannetti, Optimal control methods for quantum batteries, Phys. Rev. A **107**, 032218 (2023).

[18] A. C. Santos, B. Cakmak, S. Campbell, and N. T. Zinner, Stable adiabatic quantum batteries, Phys. Rev. E **100**, 032107 (2019).

[19] J. Monsel, M. Fellous-Asiani, B. Huard, and A. Auffèves, The energetic cost of work extraction, Phys. Rev. Lett. **124**, 130601 (2020).

[20] D. Rossini, G. M. Andolina, D. Rosa, M. Carrega, and M. Polini, Quantum advantage in the charging process of Sachdev-Ye-Kitaev batteries, Phys. Rev. Lett. **125**, 236402 (2020).

[21] K. Ito and G. Watanabe, Collectively enhanced high-power and high-capacity charging of quantum batteries via quantum heat engines, arXiv:2008.07089.

[22] A. Crescente, M. Carrega, M. Sassetti, and D. Ferraro, Ultrafast charging in a two-photon Dicke quantum battery, Phys. Rev. B **102**, 245407 (2020).

[23] J. Chen, L. Zhan, L. Shao, X. Zhang, Y. Zhang, and X. Wang, Charging quantum batteries with a general harmonic driving field, Ann. Phys. (NY) **532**, 1900487 (2020).

[24] D. Rosa, D. Rossini, G. M. Andolina, M. Polini, and M. Carrega, Ultra-stable charging of fast-scrambling SYK quantum batteries, J. High Energ. Phys. 11 (2020) 067.

[25] L. F. C. Moraes, A. Saguia, A. C. Santos, and M. S. Sarandy, Charging power and stability of always-on transitionless driven quantum batteries, Europhys. Lett. **136**, 23001 (2021).

[26] L. Peng, W.-B. He, S. Chesi, H.-Q. Lin, and X.-W. Guan, Lower and upper bounds of quantum battery power in multiple central spin systems, Phys. Rev. A **103**, 052220 (2021).

[27] F.-Q. Dou, Y.-J. Wang, and J.-A. Sun, Closed-loop three-level charged quantum battery, Europhys. Lett. **131**, 43001 (2020).

[28] F.-Q. Dou, Y.-J. Wang, and J.-A. Sun, Highly efficient charging and discharging of three-level quantum batteries through shortcuts to adiabaticity, Front. Phys. **17**, 31503 (2022).

[29] A. C. Santos, A. Saguia, and M. S. Sarandy, Stable and charge-switchable quantum batteries, Phys. Rev. E **101**, 062114 (2020).

[30] S.-F. Qi and J. Jing, Magnon-mediated quantum battery under systematic errors, Phys. Rev. A **104**, 032606 (2021).

[31] T. K. Konar, L. G. C. Lakkaraju, S. Ghosh, and A. Sen(De), Quantum battery with ultracold atoms: Bosons versus fermions, Phys. Rev. A **106**, 022618 (2022).

[32] S. Ghosh, T. Chanda, and A. Sen(De), Enhancement in the performance of a quantum battery by ordered and disordered interactions, Phys. Rev. A **101**, 032115 (2020).

[33] F. Zhao, F.-Q. Dou, and Q. Zhao, Quantum battery of interacting spins with environmental noise, Phys. Rev. A **103**, 033715 (2021).

[34] F. Zhao, F.-Q. Dou, and Q. Zhao, Charging performance of the Su-Schrieffer-Heeger quantum battery, Phys. Rev. Res. **4**, 013172 (2022).
[35] F.-Q. Dou, Y.-J. Wang, and J.-A. Sun, Charging advantages of Lipkin-Meshkov-Glick quantum battery, arXiv:2208.04831.
[36] Y. Huangfu and J. Jing, High-capacity and high-power collective charging with spin chargers, Phys. Rev. E **104**, 024129 (2021).
[37] M. B. Arjmandi, H. Mohammadi, and A. C. Santos, Enhancing self-discharging process with disordered quantum batteries, Phys. Rev. E **105**, 054115 (2022).
[38] T. F. F. Santos, Y. V. de Almeida, and M. F. Santos, Vacuum-enhanced charging of a quantum battery, Phys. Rev. A **107**, 032203 (2023).
[39] R. R. Rodríguez, B. Ahmadi, P. Mazurek, S. Barzanjeh, R. Alicki, and P. Horodecki, Catalysis in charging quantum batteries, Phys. Rev. A **107**, 042419 (2023).
[40] F.-Q. Dou, Y.-Q. Lu, Y.-J. Wang, and J.-A. Sun, Extended Dicke quantum battery with interatomic interactions and driving field, Phys. Rev. B **105**, 115405 (2022).
[41] F.-Q. Dou and F.-M. Yang, Superconducting transmon qubit-resonator quantum battery, Phys. Rev. A **107**, 023725 (2023).
[42] W.-X. Guo, F.-M. Yang, and F.-Q. Dou, Analytically solvable many-body Rosen-Zener quantum battery, Phys. Rev. A **109**, 032201 (2024).
[43] Y. Yao and X. Q. Shao, Stable charging of a Rydberg quantum battery in an open system, Phys. Rev. E **104**, 044116 (2021).
[44] W.-L. Song, H.-B. Liu, B. Zhou, W.-L. Yang, and J.-H. An, Remote charging and degradation suppression for the quantum battery, Phys. Rev. Lett. **132**, 090401 (2024).
[45] L. Fusco, M. Paternostro, and G. De Chiara, Work extraction and energy storage in the Dicke model, Phys. Rev. E **94**, 052122 (2016).
[46] S. Imai, O. Gühne, and S. Nimmrichter, Work fluctuations and entanglement in quantum batteries, Phys. Rev. A **107**, 022215 (2023).
[47] M. B. Arjmandi, A. Shokri, E. Faizi, and H. Mohammadi, Performance of quantum batteries with correlated and uncorrelated chargers, Phys. Rev. A **106**, 062609 (2022).
[48] F.-Q. Dou, H. Zhou, and J.-A. Sun, Cavity Heisenberg-spin-chain quantum battery, Phys. Rev. A **106**, 032212 (2022).
[49] K. V. Hovhannisyan, M. Perarnau-Llobet, M. Huber, and A. Acín, Entanglement generation is not necessary for optimal work extraction, Phys. Rev. Lett. **111**, 240401 (2013).
[50] F. H. Kamin, F. T. Tabesh, S. Salimi, and A. C. Santos, Entanglement, coherence, and charging process of quantum batteries, Phys. Rev. E **102**, 052109 (2020).
[51] M. Gumberidze, M. Kolář, and R. Filip, Measurement induced synthesis of coherent quantum batteries, Sci. Rep. **9**, 19628 (2019).
[52] K. Sen and U. Sen, Local passivity and entanglement in shared quantum batteries, Phys. Rev. A **104**, L030402 (2021).
[53] J.-X. Liu, H.-L. Shi, Y.-H. Shi, X.-H. Wang, and W.-L. Yang, Entanglement and work extraction in the central-spin quantum battery, Phys. Rev. B **104**, 245418 (2021).
[54] J.-Y. Gyhm, D. Šafránek, and D. Rosa, Quantum charging advantage cannot be extensive without global operations, Phys. Rev. Lett. **128**, 140501 (2022).
[55] F. Centrone, L. Mancino, and M. Paternostro, Charging batteries with quantum squeezing, Phys. Rev. A **108**, 052213 (2023).
[56] M.-L. Song, L.-J. Li, X.-K. Song, L. Ye, and D. Wang, Environment-mediated entropic uncertainty in charging quantum batteries, Phys. Rev. E **106**, 054107 (2022).
[57] S. Julià-Farré, T. Salamon, A. Riera, M. N. Bera, and M. Lewenstein, Bounds on the capacity and power of quantum batteries, Phys. Rev. Res. **2**, 023113 (2020).
[58] G. Francica, F. C. Binder, G. Guarnieri, M. T. Mitchison, J. Goold, and F. Plastina, Quantum coherence and ergotropy, Phys. Rev. Lett. **125**, 180603 (2020).
[59] G. Francica, Quantum correlations and ergotropy, Phys. Rev. E **105**, L052101 (2022).
[60] G. Francica, J. Goold, F. Plastina, and M. Paternostro, Daemonic ergotropy: Enhanced work extraction from quantum correlations, npj Quantum Inf. **3**, 12 (2017).
[61] D. Šafránek, D. Rosa, and F. C. Binder, Work extraction from unknown quantum sources, Phys. Rev. Lett. **130**, 210401 (2023).
[62] X. Yang, Y.-H. Yang, M. Alimuddin, R. Salvia, S.-M. Fei, L.-M. Zhao, S. Nimmrichter, and M.-X. Luo, Battery capacity of energy-storing quantum systems, Phys. Rev. Lett. **131**, 030402 (2023).
[63] S. Tirone, R. Salvia, S. Chessa, and V. Giovannetti, Work extraction processes from noisy quantum batteries: The role of nonlocal resources, Phys. Rev. Lett. **131**, 060402 (2023).
[64] A. Crescente, M. Carrega, M. Sassetti, and D. Ferraro, Charging and energy fluctuations of a driven quantum battery, New J. Phys. **22**, 063057 (2020).
[65] A. Delmonte, A. Crescente, M. Carrega, D. Ferraro, and M. Sassetti, Characterization of a two-photon quantum battery: Initial conditions, stability and work extraction, Entropy **23**, 612 (2021).
[66] W. Lu, J. Chen, L.-M. Kuang, and X. Wang, Optimal state for a Tavis-Cummings quantum battery via the Bethe ansatz method, Phys. Rev. A **104**, 043706 (2021).
[67] S. Ghosh and A. Sen(De), Dimensional enhancements in a quantum battery with imperfections, Phys. Rev. A **105**, 022628 (2022).
[68] P. Lipka-Bartosik, P. Mazurek, and M. Horodecki, Second law of thermodynamics for batteries with vacuum state, Quantum **5**, 408 (2021).
[69] F. Caravelli, G. Coulter-DeWit, L. P. García-Pintos, and A. Hamma, Random quantum batteries, Phys. Rev. Res. **2**, 023095 (2020).
[70] J. Carrasco, J. R. Maze, C. Hermann-Avigliano, and F. Barra, Collective enhancement in dissipative quantum batteries, Phys. Rev. E **105**, 064119 (2022).
[71] J. Q. Quach, K. E. McGhee, L. Ganzer, D. M. Rouse, B. W. Lovett, E. M. Gauger, J. Keeling, G. Cerullo, D. G. Lidzey, and T. Virgili, Superabsorption in an organic microcavity: Toward a quantum battery, Sci. Adv. **8**, eabk3160 (2022).
[72] C.-K. Hu, J. Qiu, P. J. P. Souza, J. Yuan, Y. Zhou, L. Zhang, J. Chu, X. Pan, L. Hu, J. Li, Y. Xu, Y. Zhong, S. Liu, F. Yan, D. Tan, R. Bachelard, C. J. Villas-Boas, A. C. Santos, and D. Yu, Optimal charging of a superconducting quantum battery, Quantum Sci. Technol. **7**, 045018 (2022).
[73] J. Joshi and T. S. Mahesh, Experimental investigation of a quantum battery using star-topology nmr spin systems, Phys. Rev. A **106**, 042601 (2022).

[74] I. Wenniger, S. E. Thomas, M. Maffei, S. C. Wein, M. Pont, N. Belabas, S. Prasad, A. Harouri, A. Lemaître, I. Sagnes, N. Somaschi, A. Auffèves, and P. Senellart, Experimental analysis of energy transfers between a quantum emitter and light fields, Phys. Rev. Lett. **131**, 260401 (2023).

[75] G. Gemme, M. Grossi, D. Ferraro, S. Vallecorsa, and M. Sassetti, IBM quantum platforms: a quantum battery perspective, Batteries **8**, 43 (2022).

[76] R.-H. Zheng, W. Ning, Z.-B. Yang, Y. Xia, and S.-B. Zheng, Demonstration of dynamical control of three-level open systems with a superconducting qutrit, New J. Phys. **24**, 063031 (2022).

[77] X. Huang, K. Wang, L. Xiao, L. Gao, H. Lin, and P. Xue, Demonstration of the charging progress of quantum batteries, Phys. Rev. A **107**, L030201 (2023).

[78] K.-J. Boller, A. Imamoğlu, and S. E. Harris, Observation of electromagnetically induced transparency, Phys. Rev. Lett. **66**, 2593 (1991).

[79] M. Fleischhauer, A. Imamoglu, and J. P. Marangos, Electromagnetically induced transparency: Optics in coherent media, Rev. Mod. Phys. **77**, 633 (2005).

[80] M. O. Scully, S.-Y. Zhu, and A. Gavrielides, Degenerate quantum-beat laser: Lasing without inversion and inversion without lasing, Phys. Rev. Lett. **62**, 2813 (1989).

[81] J. Mompart and R. Corbalán, Lasing without inversion, J. Opt. B: Quantum Semiclassical Opt. **2**, R7(R) (2000).

[82] U. Gaubatz, P. Rudecki, S. Schiemann, and K. Bergmann, Population transfer between molecular vibrational levels by stimulated Raman scattering with partially overlapping laser fields. A new concept and experimental results, J. Chem. Phys. **92**, 5363 (1990).

[83] N. V. Vitanov, A. A. Rangelov, B. W. Shore, and K. Bergmann, Stimulated Raman adiabatic passage in physics, chemistry, and beyond, Rev. Mod. Phys. **89**, 015006 (2017).

[84] R. H. Dicke, Coherence in spontaneous radiation processes, Phys. Rev. **93**, 99 (1954).

[85] X. Zhang and M. Blaauboer, Enhanced energy transfer in a Dicke quantum battery, Front. Phys. **10**, 1097564 (2023).

[86] G. Gemme, G. M. Andolina, F. M. D. Pellegrino, M. Sassetti, and D. Ferraro, Off-resonant Dicke quantum battery: Charging by virtual photons, Batteries **9**, 197 (2023).

[87] C. C. Sung and C. M. Bowden, Phase transition in the multimode two- and three-level Dicke model (Green's function method), J. Phys. A **12**, 2273 (1979).

[88] A. Crubellier, S. Liberman, D. Pavolini, and P. Pillet, Superradiance and subradiance. I. Interatomic interference and symmetry properties in three-level systems, J. Phys. B **18**, 3811 (1985).

[89] A. Crubellier and D. Pavolini, Superradiance and subradiance. II. Atomic systems with degenerate transitions, J. Phys. B **19**, 2109 (1986).

[90] M. M. Cola, D. Bigerni, and N. Piovella, Recoil-induced subradiance in an ultracold atomic gas, Phys. Rev. A **79**, 053622 (2009).

[91] P. Wolf, S. C. Schuster, D. Schmidt, S. Slama, and C. Zimmermann, Observation of subradiant atomic momentum states with Bose-Einstein condensates in a recoil resolving optical ring resonator, Phys. Rev. Lett. **121**, 173602 (2018).

[92] M. Hayn, C. Emary, and T. Brandes, Phase transitions and dark-state physics in two-color superradiance, Phys. Rev. A **84**, 053856 (2011).

[93] M. Hayn, C. Emary, and T. Brandes, Superradiant phase transition in a model of three-level-Λ systems interacting with two bosonic modes, Phys. Rev. A **86**, 063822 (2012).

[94] A. Baksic, P. Nataf, and C. Ciuti, Superradiant phase transitions with three-level systems, Phys. Rev. A **87**, 023813 (2013).

[95] S. Cordero, R. López-Peña, O. Castaños, and E. Nahmad-Achar, Quantum phase transitions of three-level atoms interacting with a one-mode electromagnetic field, Phys. Rev. A **87**, 023805 (2013).

[96] J. Fan and S. Jia, Collective dynamics of the unbalanced three-level Dicke model, Phys. Rev. A **107**, 033711 (2023).

[97] J. Skulte, P. Kongkhambut, H. Keßler, A. Hemmerich, L. Mathey, and J. G. Cosme, Parametrically driven dissipative three-level Dicke model, Phys. Rev. A **104**, 063705 (2021).

[98] P. Kongkhambut, H. Keßler, J. Skulte, L. Mathey, J. G. Cosme, and A. Hemmerich, Realization of a periodically driven open three-level Dicke model, Phys. Rev. Lett. **127**, 253601 (2021).

[99] Y.-Y. Chen, J.-J. Cheng, C. Ye, and Y. Li, Enantiodetection of cyclic three-level chiral molecules in a driven cavity, Phys. Rev. Res. **4**, 013100 (2022).

[100] S. Samimi and M. M. Golshan, Characteristics of superradiant optical phases occurring in the system of nondegenerate Λ atoms and radiation that are interacting inside a nonlinear quantum cavity, Phys. Rev. A **105**, 053702 (2022).

[101] R. Lin, R. Rosa-Medina, F. Ferri, F. Finger, K. Kroeger, T. Donner, T. Esslinger, and R. Chitra, Dissipation-engineered family of nearly dark states in many-body cavity-atom systems, Phys. Rev. Lett. **128**, 153601 (2022).

[102] P. Forn-Díaz, L. Lamata, E. Rico, J. Kono, and E. Solano, Ultrastrong coupling regimes of light-matter interaction, Rev. Mod. Phys. **91**, 025005 (2019).

[103] A. E. Allahverdyan, R. Balian, and T. M. Nieuwenhuizen, Maximal work extraction from finite quantum systems, Europhys. Lett. **67**, 565 (2004).

[104] W. K. Wootters, Entanglement of formation of an arbitrary state of two qubits, Phys. Rev. Lett. **80**, 2245 (1998).

[105] C. H. Bennett, H. J. Bernstein, S. Popescu, and B. Schumacher, Concentrating partial entanglement by local operations, Phys. Rev. A **53**, 2046 (1996).

[106] L. Amico, R. Fazio, A. Osterloh, and V. Vedral, Entanglement in many-body systems, Rev. Mod. Phys. **80**, 517 (2008).

[107] J. Johansson, P. Nation, and F. Nori, Qutip 2: A python framework for the dynamics of open quantum systems, Comput. Phys. Commun. **184**, 1234 (2013).

[108] E. Wigner, On the quantum correction for thermodynamic equilibrium, Phys. Rev. **40**, 749 (1932).

[109] M. Hillery, R. O'Connell, M. Scully, and E. Wigner, Distribution functions in physics: Fundamentals, Phys. Rep. **106**, 121 (1984).

[110] Y. S. Kim and E. P. Wigner, Canonical transformation in quantum mechanics, Am. J. Phys. **58**, 439 (1990).

[111] J. Weinbub and D. K. Ferry, Recent advances in Wigner function approaches, Appl. Phys. Rev. **5**, 041104 (2018).

[112] R. J. Glauber, Coherent and incoherent states of the radiation field, Phys. Rev. **131**, 2766 (1963).

[113] K. Audenaert, J. Eisert, M. B. Plenio, and R. F. Werner, Entanglement properties of the harmonic chain, Phys. Rev. A **66**, 042327 (2002).
[114] G. Vidal, J. I. Latorre, E. Rico, and A. Kitaev, Entanglement in quantum critical phenomena, Phys. Rev. Lett. **90**, 227902 (2003).
[115] J. Eisert, M. Cramer, and M. B. Plenio, Colloquium: Area laws for the entanglement entropy, Rev. Mod. Phys. **82**, 277 (2010).
[116] T. Brandes, Excited-state quantum phase transitions in Dicke superradiance models, Phys. Rev. E **88**, 032133 (2013).
[117] M. A. Bastarrachea-Magnani, S. Lerma-Hernández, and J. G. Hirsch, Comparative quantum and semiclassical analysis of atom-field systems. I. Density of states and excited-state quantum phase transitions, Phys. Rev. A **89**, 032101 (2014).
[118] P. Pérez-Fernández and A. Relaño, From thermal to excited-state quantum phase transition: The Dicke model, Phys. Rev. E **96**, 012121 (2017).
[119] P. Das and A. Sharma, Revisiting the phase transitions of the Dicke model, Phys. Rev. A **105**, 033716 (2022).
[120] A. L. Corps and A. Relaño, Comment on "Revisiting the phase transitions of the Dicke model," Phys. Rev. A **106**, 047701 (2022).
[121] P. Das, D. S. Bhakuni, and A. Sharma, Phase transitions of the anisotropic Dicke model, Phys. Rev. A **107**, 043706 (2023).
[122] V. Oganesyan and D. A. Huse, Localization of interacting fermions at high temperature, Phys. Rev. B **75**, 155111 (2007).
[123] N. Lambert, C. Emary, and T. Brandes, Entanglement and the phase transition in single-mode superradiance, Phys. Rev. Lett. **92**, 073602 (2004).
[124] S. A. Hill and W. K. Wootters, Entanglement of a pair of quantum bits, Phys. Rev. Lett. **78**, 5022 (1997).
[125] J. T. Edwards and D. J. Thouless, Numerical studies of localization in disordered systems, J. Phys. C **5**, 807 (1972).
[126] J. Lindinger, A. Buchleitner, and A. Rodríguez, Many-body multifractality throughout bosonic superfluid and Mott insulator phases, Phys. Rev. Lett. **122**, 106603 (2019).
[127] N. Macé, F. Alet, and N. Laflorencie, Multifractal scalings across the many-body localization transition, Phys. Rev. Lett. **123**, 180601 (2019).
[128] R. J. Lewis-Swan, A. Safavi-Naini, J. J. Bollinger, and A. M. Rey, Unifying scrambling, thermalization and entanglement through measurement of fidelity out-of-time-order correlators in the Dicke model, Nat. Commun. **10**, 1581 (2019).